Using circularly polarized luminescence to probe exciton coherence in disordered helical aggregates

Frank C. Spano,[1,a)] Stefan C. J. Meskers,[2] Emanuelle Hennebicq,[3] and David Beljonne[3]
[1]*Department of Chemistry, Temple University, Beury Hall 201, Philadelphia, Pennsylvania 19122, USA*
[2]*Laboratory of Macromolecular and Organic Chemistry, Eindhoven University of Technology, P.O. Box 513, 5600 MB Eindhoven, The Netherlands*
[3]*Chemistry of Novel Materials, University of Mons-Hainaut, Place du Parc 20, B-7000 Mons, Belgium*

(Received 12 February 2008; accepted 16 May 2008; published online 8 July 2008)

Circularly polarized emission from helical MOPV4 aggregates is studied theoretically based on a Hamiltonian including excitonic coupling, exciton phonon coupling, and site disorder. The latter is modeled via a Gaussian distribution of site energies. The frequency dependence of the circularly polarized luminescence dissymmetry $g_{\mathrm{lum}}(\omega)$ contains structural information about the low-energy-neutral (excitonic) polaron from which emission originates. Near the 0-0 emission frequency, $g_{\mathrm{lum}}(\omega)$ provides a measure of the exciton coherence length, while at lower energies, in the vicinity of the sideband frequencies, $g_{\mathrm{lum}}(\omega)$ probes the polaron radius. The present work focuses on how the 0-0 dissymmetry, $g_{\mathrm{lum}}^{0\text{-}0}$, relates to the emitting exciton's coherence function, from which the coherence length is deduced. In the strong disorder limit where the exciton is localized on a single chromophore, $g_{\mathrm{lum}}^{0\text{-}0}$ is zero. As disorder is reduced and the coherence function expands, $|g_{\mathrm{lum}}^{0\text{-}0}|$ increases more rapidly than the sideband dissymmetries, resulting in a pronounced surge in $g_{\mathrm{lum}}(\omega)$ near the 0-0 transition frequency. The resulting spectral shape of $g_{\mathrm{lum}}(\omega)$ is in excellent agreement with recent experiments on MOPV4 aggregates. In the limit of very weak disorder, corresponding to the motional narrowing regime, the coherence function extends over the entire helix. In this region, $g_{\mathrm{lum}}^{0\text{-}0}$ undergoes a surprising sign reversal but only for helices which are between $n+\frac{1}{2}$ and $n+1$ complete turns ($n=0,1,\ldots$). This unusual sign change is due to the dependence of the rotational line strength on long-range exciton coherences which are also responsible for a heightened sensitivity of $g_{\mathrm{lum}}(\omega)$ to long-range excitonic coupling. © *2008 American Institute of Physics*. [DOI: 10.1063/1.2943647]

I. INTRODUCTION

Understanding the complex nature of charge and energy transfer in the organic solid state is an enduring theme in chemical physics and an essential component in designing and optimizing the rich array of organic electronic devices currently under development. Excellent model systems for understanding one-dimensional energy or charge transport are the self-assembled MOPV*n* helical aggregates which have lately received considerable attention.[1–11] The helices are composed of stacks of hydrogen-bonded dimers of triazine-functionalized OPV*n* chromophores (n=the number of phenyl groups) with chiral side groups to direct helicity. In addition to unpolarized absorption and emission spectroscopy, MOPV*n* helices admit to further interrogation using circular dichroism (CD) and circularly polarized luminescence (CPL) spectroscopies. These techniques provide a wealth of information regarding the electronic and vibrational structure of the emitting exciton.[11]

MOPV*n* dissolved in nonhydrogen bonding solvents such as dodecane form helical aggregates as the temperature is lowered below approximately 40 °C.[1–3] The main signatures of aggregation are the emergence of bisignate CD activity in the vicinity of the lowest molecular singlet transition and the appearance of a shoulder on the red side of the corresponding absorption peak. The photoluminescence (PL) spectrum is characterized by a clear vibronic progression involving the ring breathing/vinyl stretching mode at approximately 1400 cm^{-1}. Upon aggregation the PL spectrum redshifts, with the 0-0 peak intensity diminishing relative to the side band intensities. In Ref. 11 we measured the CPL dissymmetry $g_{\mathrm{lum}}(\omega)$, which is defined as $2(I_L-I_R)/(I_L+I_R)$. Here $I_{L(R)}$ is the intensity of left-handed (right-handed) circularly polarized luminescence. The spectral shape of $g_{\mathrm{lum}}(\omega)$ in aggregated MOPV4 is peculiar: $|g_{\mathrm{lum}}(\omega)|$ increases steadily with frequency throughout the spectral region encompassing the PL side bands with a sharper increase or surge near the PL origin. A general increase in $|g_{\mathrm{lum}}(\omega)|$ with frequency has also been detected in small chiral molecules[12] and polymers[13–15] with thiophene-based chromophores.

As we showed in Ref. 11 the spectral shape of $g_{\mathrm{lum}}(\omega)$ provides information on the anatomy of the emitting exciton, which is more properly described as a neutral—or excitonic—polaron. Such particles consist of a vibronic (electronic and vibrational) excitation at the center of a phonon cloud, where noncentral molecules are vibrationally but not electronically excited. The magnitude of $g_{\mathrm{lum}}(\omega)$ in the

[a)]Electronic mail: spano@temple.edu.

vicinity of the emission origin increases with the exciton coherence length, as measured with respect to the center-of-mass motion of the neutral polaron, while $g_{\mathrm{lum}}(\omega)$ at lower energies increases with the polaron radius.

In this work, we develop further the relationships between the PL and CPL dissymmetry spectra of disordered helical aggregates and the exciton coherence function introduced in Ref. 11. Generally, the spatial coherence is a complex function of the strength of the excitonic couplings, the degree of static inhomogeneous disorder, the temperature (dynamic disorder), and the strength of the vibronic coupling between the exciton-forming electronic transition and intramolecular vibrational modes. As in Ref. 11, we employ a Holstein-type Hamiltonian to account for exciton-vibrational coupling between the optical transition and the 1400 cm^{-1} progression-forming intramolecular vibrational mode. Disorder is modeled as a Gaussian distribution of site transition frequencies of width σ. To simplify the analysis, we assume a spatially uncorrelated distribution and consider the low-temperature limit, where the lowest energy exciton is entirely responsible for the emission.

Extracting information about the spatial coherence of the emitting exciton from the PL or CPL dissymmetry spectrum is possible because coherence affects different portions of the spectrum differently. In aggregate emission, the 0-0 component in the vibronic progression depends directly on the spatial coherence of the emitting exciton, in marked contrast to the side band peaks which are mainly incoherent in origin. For example, in a disorder-free H-aggregate with one molecule per unit cell, the lowest energy transition is symmetry forbidden leading to a PL vibronic progression devoid of the 0-0 component.[11,16] In this case, the emitting exciton wave function is coherent over the entire aggregate, but alternates in sign between adjacent molecules leading to a complete destructive interference in the 0-0 transition dipole moment. By contrast, no such interference is operative in the side band intensities and they can never be driven to zero. In H-aggregates, the 0-0 peak can acquire intensity with increasing disorder as the coherence length shrinks and the exciton becomes localized. Because the intensity of the (incoherent) 0-1 line only weakly increases with disorder, a comparison of the 0-0 and 0-1 PL line strengths yields the exciton coherence length that in turn, provides information on the magnitude and spatial distribution of disorder.[16] It is interesting to note that J-aggregates display contrasting behavior. Since the emitting (band-bottom) exciton wave function no longer alternates in phase, the 0-0 emission is strongly allowed, leading to superradiant emission at sufficiently low temperatures.[17–19] Adding disorder reduces the coherence length and therefore the constructive interference among the molecular emitters. Hence, unlike in H-aggregates, the 0-0 intensity diminishes with increasing disorder. Similar behavior is also observed in H-like aggregates with more than a single molecule per unit cell such as thin films and nanoaggregates of oligophenylene vinylene (OPV_n) and oligothiophene (OTn, n even) chromophores. Such molecules pack in a herringbone arrangement with at least 2 molecules in a unit cell.[20–23] Here, the lower Davydov component (alias J-band) is weakly allowed along the crystal b direction,[20,24–26] leading to b-polarized superradiant 0-0 emission[27] which *diminishes* with increasing disorder.[28–31]

In helical MOPVn aggregates, coherence affects the PL spectrum in a manner similar to the ideal linear H-aggregates described above. Coherence also profoundly impacts the CPL dissymmetry spectrum $g_{\mathrm{lum}}(\omega)$ primarily in the vicinity of the 0-0 transition, thereby providing a second method with which to extract information about the emitting exciton's spatial coherence. Understanding this phenomenon in terms of the exciton coherence function introduced in Ref. 11 is the main focus of the present work.[11] In contrast to the PL spectrum, $g_{\mathrm{lum}}(\omega)$ is extremely sensitive to long-range intermolecular interactions providing a means with which to study extended interactions and dielectric screening. In Ref. 11, we showed how truncating the excitonic coupling beyond the *sixth* nearest neighbor results in a 30% increase in $|g_{\mathrm{lum}}(\omega)|$ while the PL spectrum remains practically unchanged. This strong dependence on extended interactions exists despite a disorder-induced exciton coherence length of only a few molecules. The sensitivity of the CD spectrum in helical aggregates to long-range interactions has also been analyzed by Didraga and Knoester.[32]

A final intrigue regarding $g_{\mathrm{lum}}(\omega)$ concerns its behavior in the weak disorder limit. In analyzing disorder-free helices in a prior work, we uncovered an unusual N-dependent sign change in g_{lum} in the spectral region surrounding the 0-0 transition.[33] Here, N is the number of chromophores comprising the helical aggregate. In Ref. 33, we showed that the dissymmetry of the 0-0 transition ($g_{\mathrm{lum}}^{0\text{-}0}$) scales nonlinearly with N, changing its sign twice every complete helical turn. This surprising size dependence requires temperatures to be low enough to ensure that emission emanates from the lowest energy exciton. In what follows, we show how the N-dependent sign change in $g_{\mathrm{lum}}^{0\text{-}0}$ is closely related to a disorder-induced sign change. We also show how the sign change derives from the exciton coherence function. In Ref. 33, we assumed periodic boundary conditions, in contrast to the present work, where more realistic open boundary conditions are employed throughout. As we will show, the change to open boundary conditions does not alter the unusual behavior of $g_{\mathrm{lum}}^{0\text{-}0}$ but does induce significant changes to the sideband dissymmetries ($g_{\mathrm{lum}}^{0\text{-}\nu_t}$, $\nu_t \geqslant 1$) when the exciton coupling is weak.[33]

This paper is organized as follows. After introducing the model details in the following section, we continue in Sec. III with a summary of our experimental results obtained in Ref. 11 and a thorough analysis of the effects of disorder on the PL and CPL dissymmetry line strengths. The exciton coherence function is introduced in Sec. IV and its relationship to the spectral variables is derived. A complete analysis of the disorder-free limit is performed in Sec. V. Our findings are summarized in the final section.

II. MODEL AGGREGATES, HAMILTONIAN, AND OBSERVABLES

In solution, MOPV4 molecules with triazine headgroups dimerize through quadrupole hydrogen bonding. At suffi-

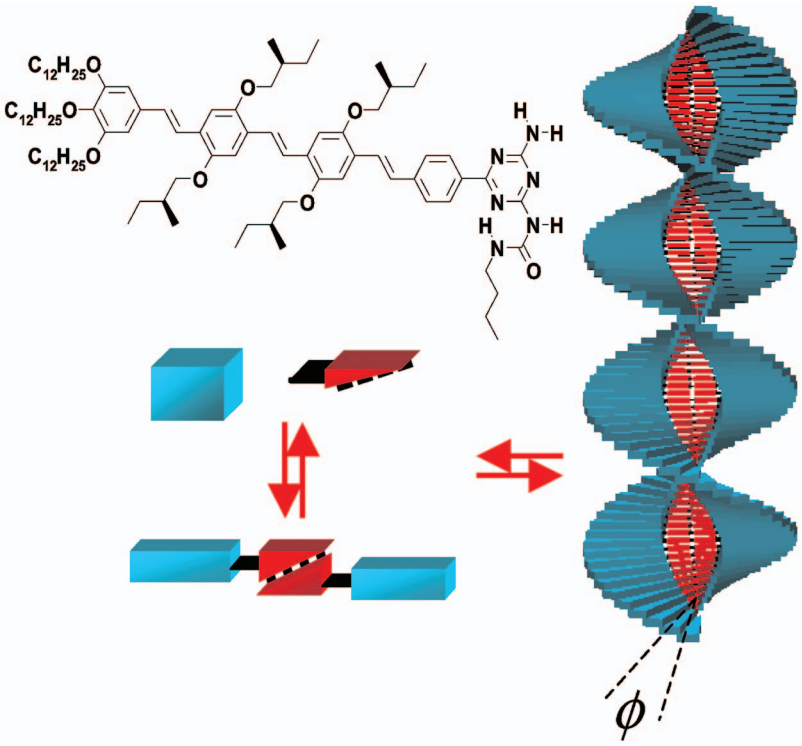

FIG. 1. (Color) Assembly of left-handed MOPV4 chiral aggregate through H-bonded dimer intermediates.

ciently low temperatures, the dimers form chiral stacks, as depicted in Fig. 1. Based on molecular dynamics simulations and the analysis of Ref. 11, the separation between the neighboring molecules d is 3.75 Å and the relative (pitch) angle between the long molecular axes in adjacent units is $\phi = 14°$, defining the left-handed helix depicted in Fig. 1.[34]

The model used to describe the photophysics of MOPV4 helices was introduced in Ref. 11. Briefly, each H-bonded dimer is associated with a single chromophoric unit, with N such units comprising the aggregate. The nth chromophore has transition frequency, $\omega_{0\text{-}0}+D+\Delta_n$, where $\omega_{0\text{-}0}+D$ is the single-site $S_0 \rightarrow S_1$ transition frequency including the gas-phase 0-0 frequency ($\omega_{0\text{-}0}$) and gas-to-crystal shift (D). The effect of disorder is manifested in Δ_n, the transition frequency offset. In our previous work,[11] Δ_n was chosen randomly from a correlated Gaussian distribution, with a spatial correlation length l_0.[35] In the numerical simulations presented here, we consider primarily the spatially uncorrelated regime ($l_0=0$) where Δ_n are chosen independently of each other. In this case, the N-body distribution function is

$$P(\Delta_1,\Delta_2,\ldots,\Delta_N) = G(\Delta_1)G(\Delta_2)\cdots G(\Delta_N), \quad l_0 = 0 \quad (1a)$$

with

$$G(\Delta_n) = \frac{1}{\sqrt{\pi}\sigma}\exp[-\Delta_n^2/\sigma^2]. \quad (1b)$$

Hence, the disorder is completely characterized by the $1/e$ full width, 2σ. The intersite correlation function takes the form, $\langle\Delta_m\Delta_n\rangle = \delta_{mn}\sigma^2/2$, i.e., is limited to the same-site variance. In the opposite regime of full correlation ($l_0=\infty$), all molecules within a given aggregate have *identical* offsets ($\langle\Delta_m\Delta_n\rangle = \sigma^2/2$), the value of which is distributed from aggregate to aggregate according to a Gaussian distribution of ($1/e$) full width, 2σ.

The localizing effects of disorder are offset by the delocalizing influence of excitonic coupling, with J_{mn} denoting the coupling between chromophores m and n. The J_{mn} for MOPV4 helices have been evaluated by semiempirical means in Ref. 11 and are shown as a function of intersite distance in Fig. 2. Based on these couplings, the free exciton bandwidth W (i.e., for inflexible molecules) is approximately 0.15 eV.

Finally, the $S_0 \rightarrow S_1$ electronic excitation within each chromophore is linearly coupled to the intramolecular ring breathing/vinyl stretching mode with frequency, $\omega_0 = 1400\ \text{cm}^{-1}$ (0.174 eV) and Huang–Rhys (HR) factor, λ^2. The latter measures the shift in the equilibrium positions of

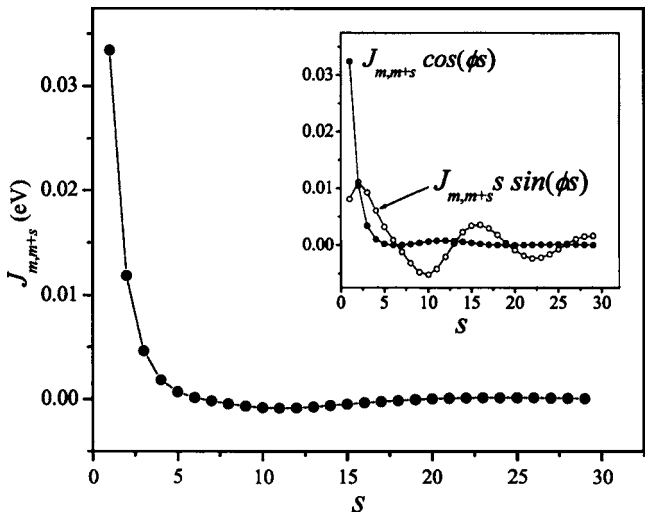

FIG. 2. The effective excitonic couplings, $J_{m,m+s}$ from Ref. 11 as a function of interchomophore distance s. The relative pitch angle is $\phi = 14°$. The inset shows the modulated couplings which appear in the spectroscopic observables.

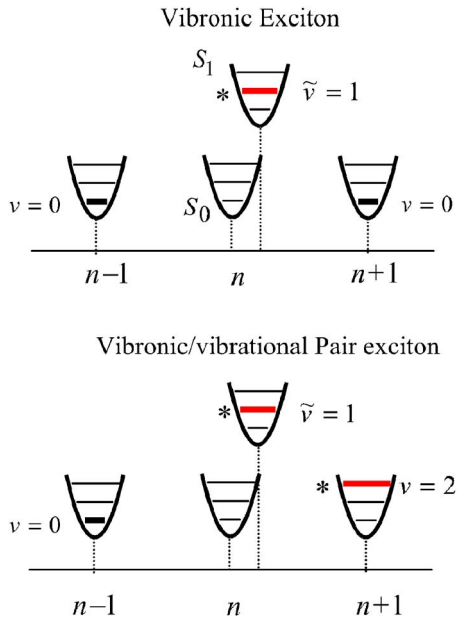

FIG. 3. (Color online) Examples of the fundamental excitations in ordered organic assemblies. The vibronic (single-particle) excitation is $|n,\tilde{\nu}=1\rangle$, while the vibronic/vibrational pair (two-particle state) is $|n,\ \tilde{\nu}=1;\ n+1,\ \nu=2\rangle$.

the ground and excited state nuclear potentials (see Fig. 3). In MOPV4, λ^2 is approximately unity, a value which, in conjunction with the cubic frequency dependence in the emission rate yields roughly equal single molecule 0-0 and 0-1 emission peak intensities, as is found for OPV4 molecules in solution.[36]

The aggregate Hamiltonian including all of the aforementioned contributions written in the subspace in which one chromophore is excited (one-exciton) is[37]

$$H=\omega_0\sum_n b_n^\dagger b_n+\omega_0\lambda\sum_n (b_n^\dagger+b_n)|n\rangle\langle n| + \sum_m\sum_n (J_{mn}+\Delta_m\delta_{mn})|m\rangle\langle n|+D+\omega_{0\text{-}0}+\lambda^2\omega_0, \quad (2)$$

where $\hbar=1$ is taken. The first term represents the vibrational energy due to the high frequency mode, while the second term represents linear exciton-phonon (EP) coupling. $b_n^\dagger(b_n)$ is the creation (destruction) operator for vibrational quanta within the harmonic ground state nuclear potential on molecule n. The pure electronic state $|n\rangle$ indicates that chromophore n is electronically excited to S_1, with all other molecules remaining in their electronic ground states (S_0). In all that follows, we employ open boundary conditions.

As described previously, the optically allowed eigenstates of H are accurately represented using one- and two-particle basis functions. In this representation, the αth exciton is[29,38]

$$|\psi^{(\alpha)}\rangle=\sum_n\sum_{\tilde{\nu}=0,1,\ldots} c_{n,\tilde{\nu}}^{(\alpha)}|n,\tilde{\nu}\rangle + \sum_n\sum_{\tilde{\nu}=0,1,\ldots}\sum_{n'}\sum_{\nu'=1,2,\ldots} c_{n,\tilde{\nu};n'\nu'}^{(\alpha)}|n,\tilde{\nu};n'\nu'\rangle. \quad (3)$$

The excitation in Eq. (3) can generally be referred to as a neutral polaron, consisting of vibronically excited one-particle states (first term) and vibronic/vibrational pair excitations or two-particle states (second term).[11] The one-particle state $|n,\tilde{\nu}\rangle$ consists of a vibronic excitation at chromophore n containing $\tilde{\nu}(=0,1,2,\ldots)$ vibrational quanta in the shifted, excited state (S_1) nuclear potential while all other molecules remain electronically and vibrationally unexcited. The two-particle state $|n,\tilde{\nu};n',\nu'\rangle$ consists of a vibronic excitation at n and a *vibrational* excitation at n' containing $\nu'(=1,2,\ldots)$ vibrational quanta in the unshifted ground state (S_0) nuclear potential.[29,38] The two excitation types are schematically shown in Fig. 3.

In order to simplify the ensuing analysis, we assume that emission originates from the lowest energy exciton, $\psi^{(\mathrm{em})}$ with transition frequency, ω_{em} within each site-disordered aggregate. Generally, $\psi^{(\mathrm{em})}$ depends on the configuration of offsets, but for notational simplicity, we suppress the subscript C. Within the low-temperature limit, the unpolarized emission intensity $S(\omega)$ consists of a vibronic progression of inhomogeneously broadened lines,

$$S(\omega)=\sum_{\nu_t=0,1,\ldots}\langle I^{0\text{-}\nu_t}(C)\omega^3\delta(\omega-\omega_{\mathrm{em}(C)}+\nu_t\omega_0)\rangle, \quad (4)$$

where $\langle\cdots\rangle$ denotes an average over randomly generated configurations (C) of site transition frequencies.[39] The configuration-dependent dimensionless line strength for the $0\text{-}\nu_t$ transition is given by

$$I^{0\text{-}\nu_t}(C)=\mu^{-2}\sum_{\{\nu_1,\nu_2,\ldots\}}{}'|\langle\psi^{(\mathrm{em})}|\hat{\boldsymbol{M}}|\{g;\nu_1,\nu_2,\ldots,\nu_N\}\rangle|^2, \quad (5)$$

where $\hat{\boldsymbol{M}}$ is the aggregate (electric) transition dipole moment (tdm) operator, consisting of a sum of radially directed molecular tdm vector operators,

$$\hat{\boldsymbol{M}}=\sum_n\hat{\boldsymbol{\mu}}_n \quad (6a)$$

with

$$\hat{\boldsymbol{\mu}}_n\equiv|n\rangle\langle g|\boldsymbol{\mu}_n+\mathrm{H.c.} \quad (6b)$$

Here, the molecular tdm, $\boldsymbol{\mu}_n=\mu[\cos(\phi n)\boldsymbol{i}-\sin(\phi n)\boldsymbol{j}]$, is directed mainly along the long axis of the nth chromophore and $|g\rangle$ is the pure electronic ground state in which all chromophores are unexcited, $|g\rangle\equiv|g_1,g_2,\ldots,g_N\rangle$, with g_n indicating molecule n in the S_0 electronic state. In Eq. (5), the terminal states in the emission process are vibrationally excited states, $|\{g;\nu_1,\nu_2,\ldots,\nu_N\}\rangle\equiv\Pi_n|g_n,\nu_n\rangle$, representing all combinations ($\{\nu_1,\nu_2,\ldots,\nu_N\}$ with $\nu_n=0,1,2\ldots$) in which a total of ν_t vibrational quanta can be distributed over all N molecules. For the $0-\nu_t$ transition, the sum in Eq. (5) is over all terminal states with the constraint, $\Sigma_n\nu_n=\nu_t$, indicated by the prime.

The CPL dissymmetry,

$$g_{\rm lum}(\omega) = \frac{1}{S(\omega)} \sum_{\nu_t=0,1,\ldots} \langle R_{\rm lum}^{0\text{-}\nu_t}(C)\omega^3 \delta(\omega - \omega_{{\rm em}(C)} + \nu_t\omega_0)\rangle \tag{7}$$

depends on the rotational line strength through the Rosenfeld equation,[40] which, for a given configuration of disorder becomes,

$$R_{\rm lum}^{0\text{-}\nu_t}(C) = \frac{4i}{c\mu^2} {\sum_{\{\nu_1,\nu_2,\ldots\}}}' \langle \psi^{(\rm em)}|\hat{\boldsymbol{M}}|\{g;\nu_1,\nu_2,\ldots\}\rangle \times \langle\{g;\nu_1,\nu_2,\ldots\}|\hat{\mathbf{m}}|\psi^{(\rm em)}\rangle. \tag{8}$$

Equation (8) includes dot products between matrix elements of the electric and magnetic dipole moment operators. The latter, denoted as $\hat{\mathbf{m}}$, is given by[33,40]

$$\hat{\boldsymbol{m}} = \frac{ick}{2}\sum_n |n\rangle\langle g|\boldsymbol{r}_n \times \boldsymbol{\mu}_n + \text{H.c.}, \tag{9}$$

where k is defined as $\omega_{\rm FC}/c$, with $\omega_{\rm FC}$ the vertical (Franck–Condon) transition frequency in the single molecule.[41] In all calculations to follow $\omega_{\rm FC}$ is taken as 2.85 eV and the nearest-neighbor distance d is 3.75 Å, as appropriate for MOPV4. These values yield $kd \approx 0.0055$.

Inserting Eq. (9) into Eq. (8) results in an alternate and physically more intuitive expression for the rotational line strength in terms of cross products of electric tdm operators,

$$R_{\rm lum}^{0\text{-}\nu_t}(C) = \frac{k}{\mu^2} {\sum_{\{\nu_1,\nu_2,\ldots\}}}' {\sum_{n,n'}}' \boldsymbol{\mu}_n^{{\rm em},\{g;\nu_1,\nu_2,\ldots\}} \times \boldsymbol{\mu}_{n'}^{\{g;\nu_1,\nu_2,\ldots\},{\rm em}} \cdot (\boldsymbol{r}_n - \boldsymbol{r}_{n'}) \tag{10}$$

with the matrix element of the site tdm operator from Eq. (6b) given by

$$\boldsymbol{\mu}_{n'}^{{\rm em},\{g;\nu_1,\nu_2,\ldots\}} \equiv \langle \psi^{(\rm em)}|\hat{\boldsymbol{\mu}}_n|\{g;\nu_1,\nu_2,\ldots,\nu_N\}\rangle. \tag{11}$$

Finally, we also define the 0-ν_t dependent dissymmetry originally introduced in Ref. 33,

$$g_{\rm lum}^{0\text{-}\nu_t} \equiv \frac{R_{\rm lum}^{0\text{-}\nu_t}}{I^{0\text{-}\nu_t}}. \tag{12}$$

When the peaks constituting the vibronic progression are narrow ($\sigma \ll \omega_0$), $g_{\rm lum}^{0\text{-}\nu_t}$ gives the dissymmetry for emission within the 0-ν_t peak.

III. NUMERICAL RESULTS FOR $g_{\rm lum}(\omega)$ AND $S(\omega)$

In this section, we present full-scale numerical simulations of the emission spectral observables in MOPV4 helices in order to establish a firm link between $g_{\rm lum}(\omega)$, $S(\omega)$, and the coherence function of the emitting exciton. We begin with Fig. 4, which summarizes our findings so far. The figure shows $g_{\rm lum}(\omega)$ from Ref. 11 for a dilute solution of MOPV4 aggregates in dodecane at $T=278$ K. The measured PL spectrum, displaying a vibronic progression involving the 1400 cm^{-1} mode, is also included for comparison. $g_{\rm lum}(\omega)$ exhibits unusual behavior, increasing steadily with energy throughout the sideband transitions with a pronounced surge in the vicinity of the 0-0 transition. To account for this behavior, we performed a detailed numerical analysis in Ref. 11 based on Eqs. (7) and (8) and Knapp's generalized distribution function allowing for variable spatial correlation lengths, l_0.[35] For example, when l_0 is zero, the transition frequencies are chosen from the Gaussian distribution of Eq. (1a) independently of one another, while for $l_0 \gg N$, all transition frequencies within a given aggregate are essentially equal (strongly correlated). The calculated spectra shown in Fig. 4 were obtained by randomly generating a given distribution of offsets and numerically diagonalizing H in Eq. (2) to obtain the one- and two-particle coefficients for the lowest energy excited state. This was done for approximately 10^4 configurations of disorder in order construct the ensemble average required in Eq. (7). The simulations in Fig. 4 also include a Boltzmann average over thermally excited emitters, although the effect of thermal averaging for the correlation lengths presented in Fig. 4 leads to only small changes ($<10\%$) in the calculated $g_{\rm lum}(\omega)$ and is not important to the current analysis.

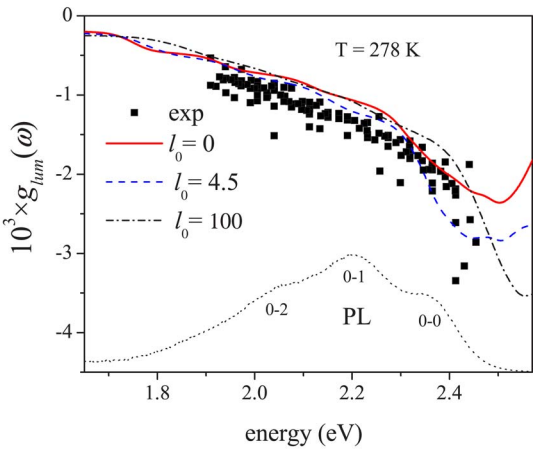

FIG. 4. (Color online) Experimental CPL dissymmetry as a function of photon energy at $T=278$ K (solid squares) for MOPV4 in dodecane from Ref. 11. Also shown are the numerically calculated dissymmetry spectra for $N=20$ aggregates with $\sigma=0.12$ eV from Ref. 11 for various spatial correlation lengths using the Hamiltonian in Eq. (2) with the interactions in Fig. 2. In addition, $\omega_0=0.174$ eV (1400 cm^{-1}), $\lambda^2=1.2$ and $\omega_{0\text{-}0}+D=2.53$ eV. Although these spectra were also averaged over a thermal distribution of emitting states ($T=278$ K), the $T=0$ K curves do not significantly differ. Dashed curve is the experimental PL spectrum from Ref. 11.

A detailed comparison of the theory and experiments summarized in Fig. 4 can be found in Ref. 11. For the purposes of the current investigation, we focus on how the calculated $g_{\rm lum}(\omega)$ evolves with increasing intra-aggregate disorder, which is associated with a decreasing spatial correlation length, l_0 in Fig. 4. Near the emission origin, the calculated $|g_{\rm lum}(\omega)|$ is strongly attenuated by disorder, in contrast to $|g_{\rm lum}(\omega)|$ in the vicinity of the sideband transitions, which is only slightly attenuated. We concluded in Ref. 11 that $|g_{\rm lum}(\omega)|$ near the emission origin is sensitive to the exciton coherence length which naturally increases with l_0. In the following section, we develop a fundamental relationship between $|g_{\rm lum}(\omega)|$ and the exciton coherence function.

A more direct way to demonstrate the link between the high-energy surge in $|g_{\rm lum}(\omega)|$ and disorder (and ultimately exciton coherence) is to plot $g_{\rm lum}(\omega)$ for various disorder

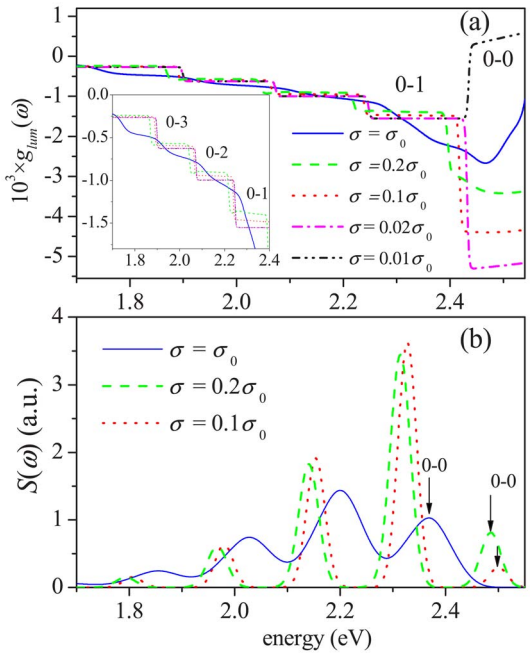

FIG. 5. (Color online) Numerically calculated CPL dissymmetry spectra (a) and PL spectra (b) for left-handed helices with $\phi=14°$ and $N=20$ chromophores at $T=0$ K. Spectra were averaged over 10^4 configurations of spatially uncorrelated site disorder for several values of σ, reported in units of $\sigma_0=0.7\omega_0$ (=0.12 eV), with the vibrational frequency set to $\omega_0=1400$ cm^{-1} (0.17 eV). Excitonic interactions are taken from Fig. 2. In evaluating the spectra using Eqs. (4) and (7), the delta function was replaced by a Gaussian homogeneous line shape function with line width, $\sigma_H=0.14\omega_0$. Thus, as the disorder width 2σ approaches zero the vibronic line widths (at $1/e$) approach $2\sigma_H$. In addition, $kd=0.0056$, $\lambda^2=1.2$ and $\omega_{0\text{-}0}+D=2.53$ eV. Arrows in (b) identify the 0-0 peaks.

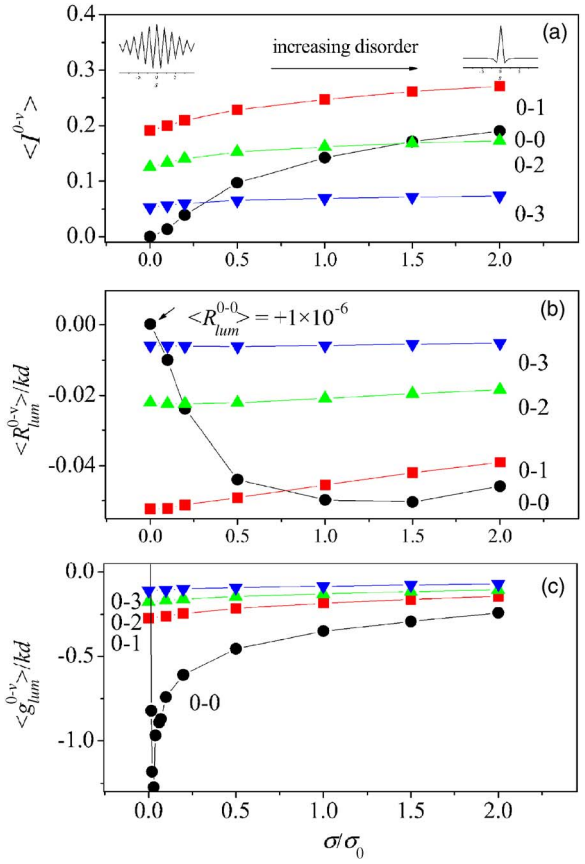

FIG. 6. (Color online) Calculated PL (a) and rotational (b) line strengths vs σ/σ_0 ($\sigma_0=0.12$ eV) for the left-handed helix ($\phi=14°$) with $N=20$ from the previous figure. In (c) the 0-ν dissymmetries are shown.

widths σ, holding l_0 constant. Figure 5 shows $g_{\text{lum}}(\omega)$ and $S(\omega)$ for several values of σ in the spatially uncorrelated ($l_0=0$) and low-temperature ($T=0$ K) limits. The disorder width is expressed in units of $\sigma_0=0.12$ eV, the value which best describes the absorption spectral broadening in MOPV4 helices.[11] Calculations were performed as described earlier. 10^4 configurations of transition offsets were chosen randomly from the distribution function in Eqs. (1a) and (1b) in order to evaluate the averages required in Eqs. (4) and (7). (No thermal averaging was performed.) The steplike behavior in $g_{\text{lum}}(\omega)$ in Fig. 5(a) arises when $\sigma \ll \omega_0$, with the midstep frequency corresponding to a vibronic peak in the PL spectrum. The step "flatness" indicates that the dissymmetry is constant throughout the vibronic peak. For the 0-ν transition, the dissymmetry is approximately

$$g_{\text{lum}}(\omega=\omega_{\text{peak}}^{0\text{-}\nu}) \approx \langle R_{\text{lum}}^{0\text{-}\nu} \rangle / \langle I^{0\text{-}\nu} \rangle \equiv \langle g_{\text{lum}}^{0\text{-}\nu} \rangle, \tag{13}$$

where $\omega_{\text{peak}}^{0\text{-}\nu}$ is the peak frequency of the 0-ν line in the PL spectrum. The approximate form [Eq. (13)] follows from Eq. (7) after assuming that (i) the line strengths and emission frequencies are uncorrelated (an excellent approximation when $l_0=0$) and (ii) $\sigma \ll \omega_0$, so that adjacent spectral lines do not significantly overlap. The redshifting of $\omega_{\text{peak}}^{0\text{-}\nu}$ with increasing disorder observed in Fig. 5(b) arises from the increased likelihood of finding lower-energy "traps" from which emission emanates. We will consider the Stokes shift in greater detail in a future publication.

Figure 5(a) portrays a striking sensitivity of $|g_{\text{lum}}(\omega)|$ to disorder near the 0–0 transition, with $\langle g_{\text{lum}}^{0\text{-}\nu} \rangle$ from Eq. (13) increasing rapidly with diminishing disorder. The behavior of $|g_{\text{lum}}(\omega)|$ with decreasing σ in Fig. 5(a) is similar to the behavior of $|g_{\text{lum}}(\omega)|$ with increasing l_0 in Fig. 4 since both decreasing σ and increasing l_0 correspond to reducing intraaggregate disorder, allowing an expansion of the exciton coherence length, as we shall see. Figure 5(a) also shows a new feature not observed in Fig. 4: in the nearly defect-free aggregate with the smallest value of σ, there is a striking sign change in $g_{\text{lum}}(\omega)$ near the 0-0 transition. In fact, a similar sign change occurs as l_0 approaches infinity for any value of σ (not shown) since in this limit aggregates become individually homogeneous.

Based on approximation [Eq. (13)] the enhancement of $|g_{\text{lum}}(\omega=\omega_{\text{peak}}^{0\text{-}0})|$ with increasing order can be understood in terms of $\langle I^{0\text{-}0} \rangle$ and $\langle R_{\text{lum}}^{0\text{-}0} \rangle$. Figure 5(b) shows that the 0-0 line strength, which is proportional to the spectral area under the 0-0 vibronic line, diminishes rapidly with increasing order, in contrast to the slight decrease experienced by the sideband line strengths. This behavior is better demonstrated in Fig. 6(a) which shows the dependence of the average line strengths $\langle I^{0\text{-}\nu} \rangle$ on σ. When no disorder is present, the 0-0 line strength is reduced to only $\approx 0.03\%$ of the single molecule value (to $3\times10^{-4}e^{-\lambda^2}$). As discussed in Ref. 16, the 0-0 line strength is rigorously zero in disorder-free achiral aggregates ($\phi=0$) due to the symmetry of the lowest energy exci-

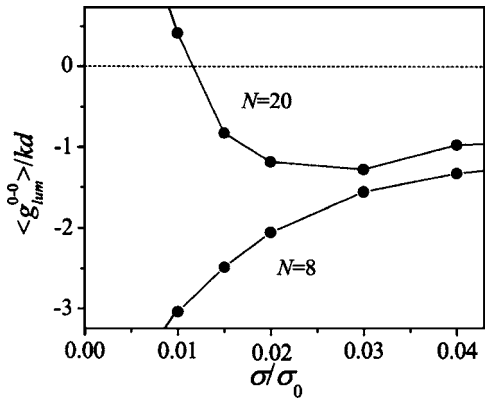

FIG. 7. Calculated 0-0 dissymmetry vs σ/σ_0 for the left-handed helix in Fig. 6 ($N=20$) in the region near the sign reversal. The 0-0 dissymmetry is also shown for a helix with $N=8$.

ton in H-aggregates. (This further assumes that the temperature is low enough to discount thermally activated emission.) As disorder increases all side band line strengths grow in intensity, although the 0-0 intensity is unique in its heightened sensitivity. In the limit of extreme disorder ($\sigma \gg W$), molecules are effectively uncoupled and all line strengths approach the single molecule values given by the FC factors,

$$I_{\mathrm{SM}}^{0\text{-}\nu} = \lambda^{2\nu} e^{-\lambda^2}/\nu!. \tag{14}$$

The enhancement of luminescence intensity with disorder has been exploited to increase the quantum yield in polymer films.[42,43]

The increase in $\langle I^{0\text{-}0} \rangle$ with increasing disorder contributes to a simultaneous decrease in $\langle g_{\mathrm{lum}}^{0\text{-}0} \rangle$ since the two quantities vary inversely with each other [see Eq. (13)]. However, $\langle g_{\mathrm{lum}}^{0\text{-}0} \rangle$ also scales directly with the rotational line strength, $\langle R_{\mathrm{lum}}^{0\text{-}0} \rangle$. The variation of all rotational line strengths $\langle R_{\mathrm{lum}}^{0\text{-}\nu} \rangle$ with disorder is shown in Fig. 6(b). As was the case for the PL line strengths, the 0-0 component is unique in its elevated sensitivity to disorder. All rotational strengths approach zero in the limit of extreme disorder, since the chirality is intermolecular in nature. This is most easily seen for $\langle R_{\mathrm{lum}}^{0\text{-}0} \rangle$ and $\langle R_{\mathrm{lum}}^{0\text{-}1} \rangle$, although the disorder would have to be much higher than the maximum value ($2\sigma_0$) in Fig. 6(b) to fully appreciate this limit. As disorder decreases throughout the window present in Fig. 6(b) the sideband rotational line strengths increase slightly in magnitude, stabilizing at their disorder-free values (see Sec. V). The behavior of $\langle R_{\mathrm{lum}}^{0\text{-}0} \rangle$ is quite different; its magnitude plummets to very low values in the weak disorder regime, with $\langle R_{\mathrm{lum}}^{0\text{-}0} \rangle$ even changing sign near $\sigma=0$. The associated behavior of $\langle g_{\mathrm{lum}}^{0\text{-}0} \rangle$ shown in Fig. 6(c) takes on a far different character since it depends on the ratio of the rotational to PL line strengths, both of which approach small values as the disorder vanishes. Because the demise of the 0-0 PL line strength outpaces that of the corresponding rotational line strength, $\langle g_{\mathrm{lum}}^{0\text{-}0} \rangle$ attains very large values as disorder vanishes. Figure 7 shows in greater detail how $\langle g_{\mathrm{lum}}^{0\text{-}0} \rangle$ behaves as σ approaches zero. After a sign reversal at approximately $0.01\sigma_0$, $\langle g_{\mathrm{lum}}^{0\text{-}0} \rangle$ climbs to $\approx 55kd=0.31$ at $\sigma=0$ (not shown). This is a substantial fraction of the theoretical maximum of 2.0 although the corresponding 0-0 PL intensity is very small. Moreover, Fig. 7 shows that the sign change is not general. For a helix with only eight chromophores there is no sign change. Further analysis of helices with $N \leqslant 20$ showed the sign change develops after $N=10$.

Unlike the 0-0 line strengths, the *sideband* line strengths are well-behaved and only weakly dependent on N. For example, for $N=8$ $\langle R_{\mathrm{lum}}^{0\text{-}\nu} \rangle$ and $\langle I^{0\text{-}\nu} \rangle$ for $\nu \geqslant 1$ match the corresponding quantities for $N=20$ except for a small discrepancy in the weak disorder regime where the $N=8$ values are slightly in excess by approximately 10%.

Through further numerical analysis, we have determined that the sign change in $\langle g_{\mathrm{lum}}^{0\text{-}0} \rangle$ along with its escalating magnitude coincides with the entry into the weak disorder or motional narrowing regime of Knapp.[35] When the disorder width σ satisfies,

$$\sigma \ll \pi^2 W e^{-\lambda^2}/N^{3/2}, \tag{15}$$

excitations are well-described as fully delocalized excitons; for example, excitons with good wave vector quantum numbers k if periodic boundary conditions are invoked. Disorder only weakly mixes such states, with first order changes strongest between the neighboring k and $k+1$ excitons. For the parameters of Fig. 6, the Knapp condition becomes $\sigma \ll 0.04\sigma_0 = 40\ \mathrm{cm}^{-1}$, corresponding to the region in Figs. 6(c) and 7 where $\langle g_{\mathrm{lum}}^{0\text{-}0} \rangle$ changes sign. In Sec. V, the unusual behavior exhibited by $\langle g_{\mathrm{lum}}^{0\text{-}0} \rangle$ in the weak disorder limit is investigated in more detail.

IV. THE EXCITON COHERENCE FUNCTION

The behavior of $S(\omega)$ and $g_{\mathrm{lum}}(\omega)$ in the spectral region surrounding the 0-0 transition can be better understood in terms of the exciton coherence function introduced in Ref. 11. For the lowest energy (emitting) exciton, the coherence function is defined as

$$C^{(\mathrm{em})}(s) \equiv \sum_n \langle \psi^{(\mathrm{em})} | B_n^+ B_{n+s} | \psi^{(\mathrm{em})} \rangle, \tag{16}$$

where B_n^+ is the local exciton creation operator, given by $B_n^+ \equiv |n;0,0,\ldots,0\rangle\langle g;0,0,\ldots,0|$. In the state $|n;0,0,\ldots,0\rangle$, molecule n is electronically excited (S_1) while all other molecules remain in the ground state, S_0. Moreover, *all* molecules (including the nth molecule) remain in the vibrational ground state relative to the unshifted (S_0) potential. $|\{g;0,0,\ldots 0\}\rangle$ is the aggregate electronic/vibrational ground state defined following Eq. (5). Note that in our definition, B_n^+ and B_n are not pure electronic operators; hence, $\Sigma_n B_n^+ B_n$ is *not* the usual exciton number operator and $C^{(\mathrm{em})}(0)$ is *not* generally unity. As we will show, with the coherence function defined in Eq. (16), $C^{(\mathrm{em})}(0)$ provides useful information about the level of nuclear relaxation in the vibronically excited molecule.

Inserting the wave function [Eq. (3)] into the coherence function [Eq. (16)] shows that $C^{(\mathrm{em})}(s)$ depends only on the vibronic or single-particle components of the emitting exciton wave function,

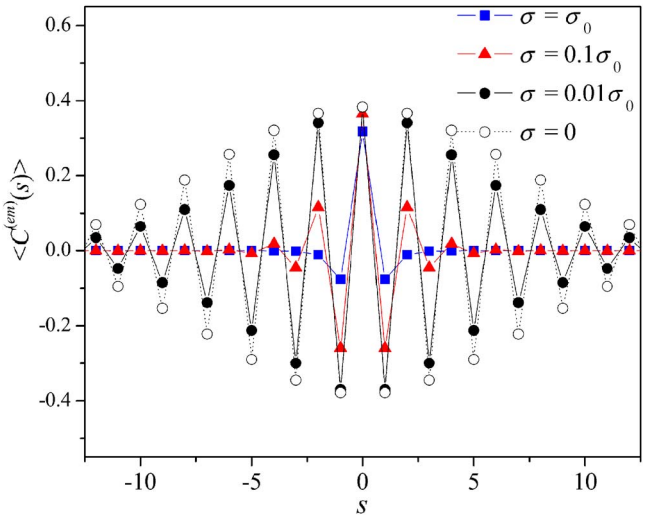

FIG. 8. (Color online) Numerically calculated exction coherence function for three values of σ from Fig. 5 using Eq. (17) and averaging over 10^4 configurations of disorder. In addition, $N=20$ and $\lambda^2=1.2$.

$$C^{(\mathrm{em})}(s)=\sum_{n}\sum_{\tilde{\nu},\tilde{\nu}'} f_{\tilde{\nu},0} f_{\tilde{\nu}',0} c^{(\mathrm{em})}_{n,\tilde{\nu}} c^{(\mathrm{em})}_{n+s,\tilde{\nu}'}, \tag{17}$$

where the overlap between the harmonic oscillator eigenfunction with $\tilde{\nu}$ quanta in the shifted (S_1) potential and that with ν quanta in the unshifted (S_0) potential is given by, $f_{\tilde{\nu},\nu}\equiv\langle\tilde{\nu}|\nu\rangle$ (see Fig. 3). For harmonic wells, $f_{\tilde{\nu},0}\equiv\lambda^{\tilde{\nu}}\exp(-\lambda^2/2)/\sqrt{\tilde{\nu}!}$.

Figure 8 shows the configurationally averaged coherence function, $\langle C^{(\mathrm{em})}(s)\rangle$, for several values of σ from Fig. 5 in a helix containing $N=20$ choromophores. Also included is the homogeneous limit, $\sigma=0$. As order increases, the exciton becomes increasingly delocalized, developing a phase alternation characteristic of the band bottom ("$k=\pi$") exciton in an ideal H-aggregate. Note the large increase in the spatial extent of the coherence function as one enters the motional narrowing regime ($\sigma<0.04\sigma_0$), where $C^{(\mathrm{em})}(s)$ extends over all N chromophores. When disorder is completely absent, the full width at half maximum of $C^{(\mathrm{em})}(s)$ is approximately N. The attenuation of $C^{(\mathrm{em})}(s)$ with increasing $|s|$ in the disorder-free limit is due to open boundary conditions, see, for example, Eq. (34) and Fig. 11. (Under periodic bound conditions, $|C^{(\mathrm{em})}(s)|$ is independent of s when disorder is absent).

In the opposite limit of extreme disorder, ($\sigma\gg W$), $\langle C^{(\mathrm{em})}(s)\rangle$ approaches $\exp(-\lambda^2)\delta_{s0}$ as the excitation localizes on a single chromophore. The exponential factor indicates that the electronic excitation is fully relaxed in the *shifted* nuclear well with $\tilde{\nu}=0$ vibrational quanta (see Fig. 3). The increase in $\langle C^{(\mathrm{em})}(0)\rangle$ beyond $\exp(-\lambda^2)$ with decreasing disorder observed in Fig. 8 indicates that the vibronically excited molecule is no longer fully relaxed in the shifted (S_1) potential. When disorder vanishes entirely, $\langle C^{(\mathrm{em})}(0)\rangle$ is determined by the ratio, $W/\lambda^2\omega_0$: for strong excitonic coupling ($W\gg\lambda^2\omega_0$), $\langle C^{(\mathrm{em})}(0)\rangle$ increases to unity as the emitting exciton evolves towards a free exciton. In the opposite regime ($W\ll\lambda^2\omega_0$) $\langle C^{(\mathrm{em})}(0)\rangle$ remains at $\exp(-\lambda^2)$.

The relationship between the emission spectrum and $\langle C^{(\mathrm{em})}(s)\rangle$ can be appreciated by first noting that the (average) 0-0 line strength is obtained by integrating just the 0-0 component ($\nu_t=0$ term) of $S(\omega)$ in Eq. (4)—call it $S^{0\text{-}0}(\omega)$—over frequency ω

$$\int \omega^{-3} S^{0\text{-}0}(\omega)\,d\omega=\langle I^{0\text{-}0}\rangle. \tag{18a}$$

The 0-0 line strength is, in turn, related to the exciton coherence function,

$$\langle I^{0\text{-}0}\rangle=\sum_{s}\langle C^{(\mathrm{em})}(s)\rangle\cos(\phi s), \tag{18b}$$

as can be seen by comparing the definition of the 0-0 line strength in Eq. (5) with the coherence function definition in Eq. (16).

Equation (18b) and Fig. 8 show how the demise in the 0-0 line strength with increasing order can be understood in terms of the coherence function for the emitting exciton. As the coherence function expands with increasing order, the sum in Eq. (18b) is more effectively canceled leading to the diminishing 0-0 line strength observed in Figs. 5(b) and 6.[11] In the limit of no disorder ($\sigma=0$), the 0-0 line strength is practically zero due to a nearly complete destructive interference—it is rigorously zero only when the helical pitch angle ϕ is also zero. In *J*-aggregates, the coherence function for the band-bottom exciton does not oscillate in sign; hence, the sum in Eq. (18b) represents constructive interference, leading to an N-fold enhancement and superradiance.[17–19]

The very different behavior exhibited by the side-band line strengths ($I^{0\text{-}1}, I^{0\text{-}2},\ldots$)—i.e., their weak dependence on σ observed in Fig. 6 — arises because they are not dependent on the exciton coherence function and consequently they cannot be driven to zero via destructive interference. Rather, they depend on *incoherent* sums involving one- and two-particle coefficients.[28,29,31] For example, the 0-1 PL line strength obtained by inserting the emitting exciton wave function [Eq. (3)] into Eq. (5) is given by

$$\langle I^{0\text{-}1}\rangle=\sum_{n}\left\langle\left|\sum_{\tilde{\nu}} f_{\tilde{\nu},1} c^{(\mathrm{em})}_{n,\tilde{\nu}}+\sum_{n',\tilde{\nu}} f_{\tilde{\nu},0} c^{(\mathrm{em})}_{n',\tilde{\nu};n1} e^{i\phi(n-n')}\right|^2\right\rangle. \tag{19}$$

As we showed in Ref. 16 for the achiral P3HT π-stack, the interference between one- and two-particle terms occurring in Eq. (19) leads to diminished sideband intensities with increasing exciton bandwidth, the basis for the well-documented observation of aggregation-induced fluorescence quenching.[42,43] Furthermore, in the limit of extreme disorder and weak excitonic coupling ($\sigma\gg\lambda^2\omega_0>W$), Eq. (19) reduces to the single molecule value of $\lambda^2\exp(-\lambda^2)$. This follows because $c^{(\mathrm{em})}_{n,\nu}$ approaches $\delta_{n,\bar{n}}\delta_{\tilde{\nu},0}$ and the two-particle coefficients approach zero as localization proceeds to trap the excitation at position $\bar{n}$.

The exciton coherence function also accounts for the unusual behavior exhibited by $g_{\mathrm{lum}}(\omega)$ near the emission origin. In order to express $\langle g^{0\text{-}0}_{\mathrm{lum}}\rangle$ in terms of the coherence function, we need to find first how $\langle R^{0\text{-}0}_{\mathrm{lum}}\rangle$ depends on $\langle C^{(\mathrm{em})}(s)\rangle$ and then divide the result by $\langle I^{0\text{-}0}\rangle$ from Eq. (18b). Using Eqs. (3), (8), and (16), we obtain

$$\langle R_{\mathrm{lum}}^{0\text{-}0}\rangle = kd\sum_{s}\langle C^{(\mathrm{em})}(s)\rangle s\,\sin(\phi s). \tag{20}$$

$\langle R_{\mathrm{lum}}^{0\text{-}0}\rangle$ also depends on a sum over the exciton coherence function but modulated by $s\sin(\phi s)$ instead of $\cos(\phi s)$ as in $\langle I^{0\text{-}0}\rangle$. Hence, $\langle C^{(\mathrm{em})}(s=0)\rangle$ does not contribute to the sum in Eq. (20) causing $\langle R_{\mathrm{lum}}^{0\text{-}0}\rangle$ and therefore $\langle g_{\mathrm{lum}}^{0\text{-}0}\rangle$ to vanish in the limit of a strong disorder. The vanishing of $\langle g_{\mathrm{lum}}^{0\text{-}0}\rangle$ under strong disorder conditions is strictly valid when the individual chromophores are achiral as we have assumed in our model. In reality, the chirality of the MOPV4 molecules of Fig. 1 contributes a small, nonresonant molecular component to the rotational strength which is neglected in our model.

As disorder decreases away from the strong disorder limit, $|\langle R_{\mathrm{lum}}^{0\text{-}0}\rangle|$ initially increases from zero as the exciton coherence length expands [see Fig. 6(b)]. Eventually, however, the destructive interference inherent in Eq. (20) causes $|\langle R_{\mathrm{lum}}^{0\text{-}0}\rangle|$ to diminish, but more gradually than $\langle I^{0\text{-}0}\rangle$ due to the longer range of the $s\sin(\phi s)$ modulation compared with $\cos(\phi s)$. Upon entering the motional narrowing regime, the coherence length approaches the physical length of the helix, as depicted in the inset of Fig. 8. Because the destructive interference is more effective in $\langle I^{0\text{-}0}\rangle$ than in $\langle R_{\mathrm{lum}}^{0\text{-}0}\rangle$, the magnitude of the ratio, $|\langle g_{\mathrm{lum}}^{0\text{-}0}\rangle|$, increases rather dramatically as σ approaches zero. As depicted in Fig. 6(c), there may even be a sign change in $\langle g_{\mathrm{lum}}^{0\text{-}0}\rangle$ prior to its escalating magnitude, a purely coherent effect ultimately deriving from the long-range modulation of $\langle R_{\mathrm{lum}}^{0\text{-}0}\rangle$ in Eq. (20). In the next section, the relationship between the sign change and N is derived.

In contrast to the 0-0 dissymmetry, the sideband dissymmetries [see Fig. 5(a)] depend on a product of one- and two-particle coefficients and, therefore, cannot be expressed solely in terms of the exciton coherence function.[11,33] For example, the 0-1 dissymmetry, using Eqs. (3), (8), and (12), is given by

$$\begin{aligned}\langle g_{\mathrm{lum}}^{0\text{-}1}\rangle = {} & \frac{2kd}{\langle I^{0\text{-}1}\rangle}\sum_{n_1,n_2}\sum_{\tilde{\nu},\tilde{\nu}'} f_{\tilde{\nu},1}f_{\tilde{\nu}',0}\langle c^{(\mathrm{em})}_{n_1,\tilde{\nu}}c^{(\mathrm{em})}_{n_2,\tilde{\nu}';n_1 1}\rangle \\ & \times(n_1-n_2)\sin\phi(n_1-n_2) \\ & + \frac{kd}{\langle I^{0\text{-}1}\rangle}\sum_{n}\sum_{n_1,n_2}\sum_{\tilde{\nu},\tilde{\nu}'} f_{\tilde{\nu},0}f_{\tilde{\nu}',0}\langle c^{(\mathrm{em})}_{n_1,\tilde{\nu};n1}c^{(\mathrm{em})}_{n_2,\tilde{\nu}';n1}\rangle \\ & \times(n_1-n_2)\sin\phi(n_1-n_2). \end{aligned} \tag{21}$$

Were it not for vibronic/vibrational pair contributions in Eq. (21), the sideband dissymmetries would rigorously vanish. Moreover, as shown in Ref. 11, the two-particle coefficients appearing in Eq. (21) are directly responsible for the magnitude of the vibrational excitations on chromophores *other* than the electronically excited one. Hence, $|g_{\mathrm{lum}}^{0\text{-}\nu_t}|$ with $\nu_t>0$ provides a measure of the polaron radius, as emphasized in our previous work.[11]

V. DISORDER-FREE AGGREGATES

In order to account for the unusual behavior exhibited by $g_{\mathrm{lum}}(\omega)$ in the weak disorder limit, we derive in this section analytical expressions for the spectral line strengths in homogeneous (disorder-free) helices. To simplify the analysis, we work in the weak excitonic coupling (alias strong EP coupling) regime, $W\ll\omega_0\lambda^2$. Although the limit is approximate for MOPVn aggregates, where the free exciton bandwidth $W\approx 0.15$ eV is only slightly smaller than the vibrational relaxation energy, $\omega_0\lambda^2\approx 0.17$ eV, we will find that $g_{\mathrm{lum}}^{0\text{-}0}$ calculated perturbatively remains surprisingly accurate. The weak exciton coupling limit was originally explored in Ref. 33 using periodic boundary conditions and nearest-neighbor only coupling. In the latter part of this section, we revisit this regime using the more physically relevant open boundary conditions and include the effects of extended excitonic coupling.

For weak excitonic coupling, single-particle states $|n,\tilde{\nu}\rangle$ are organized into vibronic bands characterized by the number of vibrational excitations in the relaxed, excited state nuclear potential, $\tilde{\nu}$.[16] Since states within a given vibronic band are degenerate when $W=0$, the correct zero order states must first be identified. In the vibronic band with $\tilde{\nu}$ $(=0,1,2,\ldots)$ vibrations, the zero order states are delocalized single-particle excitons or vibrons[16]

$$|k,\tilde{\nu}\rangle^{(0)} = \sum_{n}\phi_{k,n}|n;\tilde{\nu}\rangle, \tag{22}$$

where the coefficients $\phi_{k,n}$ for the kth eigenstate are found by diagonalizing the excitonic part of the Hamiltonian [third term in Eq. (2)]. The form of $\phi_{k,n}$ for the case of nearest-neighbor only coupling is given below.

The first order corrections to the low-energy excitons include a term comprised entirely of vibronic excitons, and a vibronic/vibrational pair (two-particle) term. If we generalize the wave function from Ref. 16 to include extended excitonic couplings, we obtain the wave functions in the $\tilde{\nu}=0$ band correct to first order[16,44]

$$\begin{aligned}|k,\tilde{\nu}=0\rangle = {} & |k,\tilde{\nu}=0\rangle^{(0)} - \frac{\tilde{J}_k}{\omega_0}\sum_{\tilde{\nu}'\geq 1}\frac{f_{\tilde{0}0}f_{\tilde{\nu}'0}}{\tilde{\nu}'}|k,\tilde{\nu}'\rangle^{(0)} \\ & - \sum_{n,\tilde{\nu}'\geq 0}\sum_{m,\nu'\geq 1}\frac{J_{n,m}f_{\tilde{\nu}'0}f_{\tilde{0}\nu'}\phi_{k,m}}{(\tilde{\nu}'+\nu')\omega_0}|n,\tilde{\nu}';m,\nu'\rangle \end{aligned} \tag{23}$$

with the k-dependent excitonic sums given by, $\tilde{J}_k \equiv \Sigma_{m,n}\phi^*_{k,n}\phi_{k,m}J_{n,m}$. The second term is an interband term[16] since it involves coupling to states in higher vibronic bands with the same k. The (third) two-particle term is written in a localized basis set in order not to introduce additional notation for extended two-particle states. We have recently utilized the wave function [Eq. (23)] in order to successfully analyze absorption and emission in P3HT π-stacks.[16,44,45]

The emitting state is the lowest energy state in the $\tilde{\nu}=0$ band. It is denoted as $|\bar{k},\tilde{\nu}=0\rangle$, where $\bar{k}$ minimizes the first order energy,

$$\omega_k = \omega_{0\text{-}0} + D + e^{-\lambda^2}\tilde{J}_k. \tag{24}$$

For the H-like aggregates treated here $\bar{k}$ is such that the wave function coefficients $\phi_{\bar{k},m}$ change sign every molecule. Inserting the wave function $|\bar{k},\tilde{\nu}=0\rangle$ from Eq. (23) for the

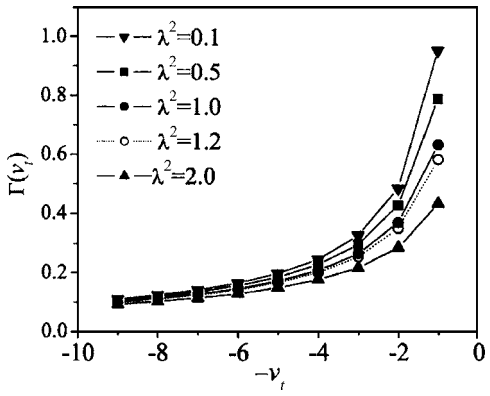

FIG. 9. The behavior of $\Gamma(\nu_t)$ from Eq. (30) as a function of $-\nu_t$ for several HR parameters.

emitting exciton into Eq. (5) for the 0-0 PL line strength gives

$$I^{0\text{-}0} = \sum_s C^{(\mathrm{em})}(s)\cos(\phi s) + O[(W/\omega_0)] \tag{25}$$

with the exciton coherence function given by

$$C^{(\mathrm{em})}(s) = e^{-\lambda^2}\sum_n \phi^-_{k,n}\phi^-_{k,n+s}. \tag{26}$$

By contrast, the sideband intensities are not coherently enhanced and remain close to the single molecule values,

$$I^{0\text{-}\nu_t} \approx I^{0\text{-}\nu_t}_{\mathrm{SM}} + O[W/\omega_0], \quad \nu_t \geqslant 1 \tag{27}$$

with $I^{0\text{-}\nu_t}_{\mathrm{SM}}$ given in Eq. (14).

As before, the uniqueness of the 0-0 component in the PL vibronic progression becomes apparent. Figure 10(b) shows how the 0-0 line strength $I^{0\text{-}0}$ decreases steadily with N from $\approx$1% of the isolated molecule value at $N=4$ to about 0.001% at $N=20$. The demise with N is due to the destructive interference embodied in the sum of the coherence function in Eq. (26). Although not shown the side band PL line strengths are only weakly dependent on N consistent with the zero order result in Eq. (27).

A substantial disparity between the fundamental and sideband components is also expected for the CPL dissymmetry. After insertion of the first order wave function [Eq. (23)] into Eq. (8) and subsequent use of Eqs. (26) and (12), we obtain

$$g^{0\text{-}0}_{\mathrm{lum}} = \frac{kd}{I^{0\text{-}0}}\sum_s C^{(\mathrm{em})}(s)s\,\sin(\phi s) + \mathrm{O}[W/\omega_0] \tag{28}$$

for the 0-0 dissymmetry with $I^{0\text{-}0}$ taken from Eq. (25) and

$$g^{0\text{-}\nu_t}_{\mathrm{lum}} = -2kd\Gamma(\nu_t)\omega_0^{-1}\sum_{m,s}(\phi^-_{k,m})^2 J_{m,m+s}s\,\sin(\phi s) + \mathrm{O}[(W/\omega_0)^2], \quad \nu_t \geqslant 1 \tag{29}$$

for the sideband dissymmetries. In Eq. (29), the effects of vibronic coupling are contained in the function,

$$\Gamma(\nu_t) \equiv \sum_{\tilde{\nu}=0,1\ldots}\frac{e^{-\lambda^2}\lambda^{2\tilde{\nu}}}{(\tilde{\nu}+\nu_t)\tilde{\nu}!}. \tag{30}$$

Figure 9 shows the dependence of $\Gamma(\nu_t)$ on $-\nu_t$, for several HR factors. Figure 9 explains the steady rise of $|g_{\mathrm{lum}}(\omega)|$ with frequency observed in the measurements of Fig. 4 (recall the emission frequency increases with $-\nu_t\omega_0$).

The differences between the fundamental and sideband dissymmetries contained in Eqs. (28) and (29) is quite profound. The 0-0 dissymmetry is largely independent of exciton bandwidth W,[33] while the side band dissymetries scale directly with the coupling strengths, J_{mn}. $g^{0\text{-}0}_{\mathrm{lum}}$ is also independent of vibronic coupling since the exponential factor in the coherence function of Eq. (28) is exactly canceled by the same factor appearing in the 0-0 line strength in Eq. (25). Conversely, the side band dissymmetries depend on the vibronic coupling through $\Gamma(\nu_t)$. It is quite surprising that $g^{0\text{-}0}_{\mathrm{lum}}/kd$ depends only on N and ϕ, i.e., a free exciton displays the same 0-0 dissymmetry as a dressed polaron.

The sideband dissymmetries displayed in Eq. (29) are sensitive to the long-range excitonic couplings through the modulated interactions, $s\,\sin(\phi s)J_{m,m+s}$. The inset of Fig. 2 shows how the modulation enhances contributions from more distant couplings. As we show in a future publication, the $s\,\sin(\phi s)$ modulation also holds in the strong disorder regime, pointing toward a more general dependence. The enhanced sensitivity of $g^{0\text{-}\nu}_{\mathrm{lum}}$ $(\nu \geqslant 1)$ to long-range interactions has been noted in Ref. 11, where it was shown that truncating the excitonic interactions after the sixth nearest-neighbor interaction leads to a dramatic 30% decrease in $|g_{\mathrm{lum}}|$ compared to a negligible change in the emission spectrum $S(\omega)$. The latter depends on the much shorter-range cosine modulated interactions, as shown in the Fig. 2 (inset).

Figure 10 shows the various dissymmetries $g^{0\text{-}\nu_t}_{\mathrm{lum}}$ evaluated using Eqs. (28) and (29) as a function of the number of chromophores N in a homogeneous aggregate with weak excitonic coupling. The $\phi^-_{k,n}$ coefficients were obtained numerically by diagonalizing just the excitonic part of H in Eq. (2) using the extended MOPV4 interactions in Fig. 2. The sideband dissymmetries are well-behaved with N, leveling off by approximately $N=20$ to the limiting values,

$$g^{0\text{-}\nu_t}_{\mathrm{lum}} = -2kd\Gamma(\nu_t)\omega_0^{-1}\sum_s J_{m,m+s}s\,\sin(\phi s), \quad \nu_t \geqslant 1. \tag{31}$$

At $N=20$, the perturbative values in Fig. 10(a) overestimate the exact dissymmetries of Fig. 6(c) (see $\sigma=0$ points) by only $\approx$30%. Since the sideband dissymmetries only weakly depend on disorder [see Fig. 6(c)] Eq. (29) is quite robust and is able to approximately describe disordered MOP4 helices.

Unlike the sideband dissymmetries, $g^{0\text{-}0}_{\mathrm{lum}}$ varies strongly with N, exhibiting periodic behavior, as shown in the inset of Fig. 10(b). For small left-handed helices, $g^{0\text{-}0}_{\mathrm{lum}}$ is initially negative, increasing with N and changing sign between $N=10$ and 12, when the helix completes approximately $\frac{1}{2}$ turn. The unusual N-dependence of $g^{0\text{-}0}_{\mathrm{lum}}$ is due to the interference effects inherent in the sum [Eq. (28)], and is similar to what was obtained using periodic boundary conditions in Ref. 33. The large value, $g^{0\text{-}0}_{\mathrm{lum}}=+0.26$ corresponding to $N=20$ in Fig. 10(b) is in surprisingly good agreement with the exact value (0.31) obtained fully numerically in Sec. III. This follows from the aforementioned weak dependence of $g^{0\text{-}0}_{\mathrm{lum}}$ on the exciton bandwidth.

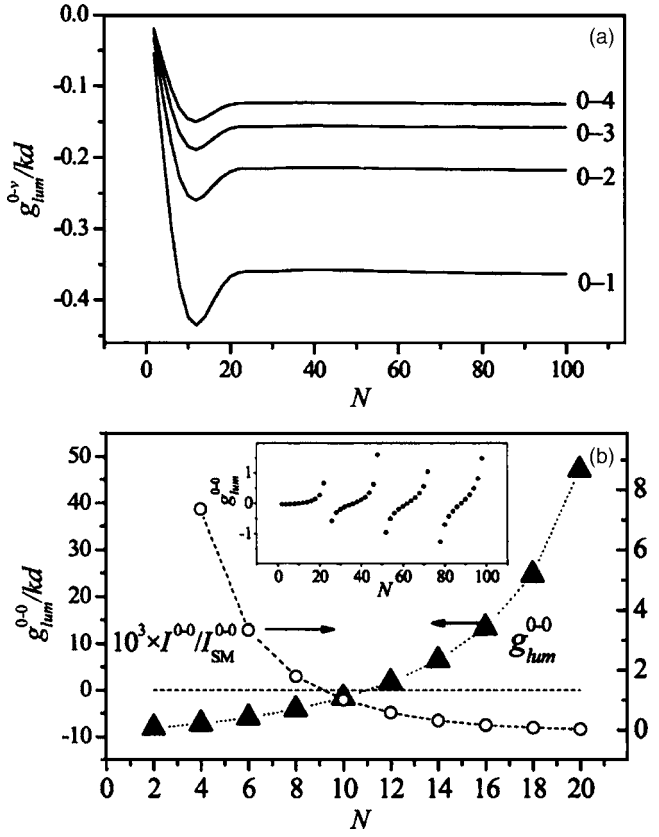

FIG. 10. The CPL sideband dissymmetries (a) and 0-0 dissymmetry (b) in defect-free left-handed helices with $\phi=14°$ as a function of the number of chromophores N in the weak excitonic coupling limit (see text). Extended interactions are taken from Fig. 2. The 0-0 and side band dissymmetries were calculated using Eqs. (28) and (29) with numerically determined coefficients $\phi_{\tilde{k}n}$ for open boundary conditions and $\lambda^2=1.2$. All other parameters are the same as in Fig. 6. The 0-0 PL line strength as a function of N from Eq. (25) is also plotted in (b). The inset in (b) shows the 0-0 dissymmetry over a much larger range of N values. Apparent divergences appear when the helix makes an integral number of complete turns according to condition (36).

Figure 10(b) shows that the disorder-induced sign change shown in Fig. 5(a) depends on N. It arises whenever $N\phi$ lies between π and 2π, modulo 2π. One can appreciate the effect as follows. When disorder is strong and the exciton is well localized over only a few chromophores, the sign of $g_{\mathrm{lum}}^{0\text{-}0}$ is negative (positive) in a left (right) handed helix, independent of the number of *chromophores* N. As disorder is reduced and the coherence length expands the sign of $g_{\mathrm{lum}}^{0\text{-}0}$ ultimately settles on the value predicted from Fig. 10(b). For example, a sign change develops in the weak disorder limit described by Eq. (15) for $N=20$ but not $N=8$ (see Fig. 7).

A. Nearest-neighbor only coupling

To better understand the complex behavior of $g_{\mathrm{lum}}^{0\text{-}0}$ in homogeneous aggregates, we turn to a simpler model in which excitonic interactions are limited to nearest neighbors. The model was originally analyzed in detail in Ref. 33, where an analytical expression for $g_{\mathrm{lum}}^{0\text{-}0}$ was derived using periodic boundary conditions. In what follows, we extend the analysis started in Ref. 33 to helical aggregates with the far more realistic open boundary conditions.

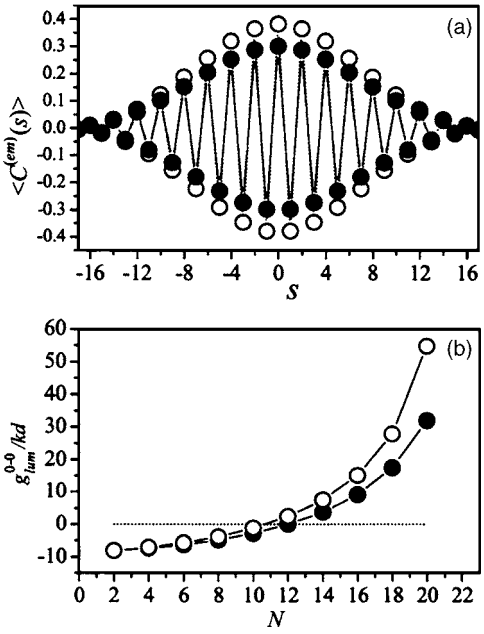

FIG. 11. (a) The exciton coherence function in Eq. (34) (solid circles) plotted alongside the coherence function for $\sigma=0$ from Fig. 7 (open circles). (b) The corresponding 0-0 CPL dissymmetries as a function of the number of chromophores N.

When nearest-neighbor only interactions are included, the zero order vibronic wave function coefficients from Eq. (22) are

$$\phi_{k,n}=\sqrt{\frac{2}{N+1}}\sin\left(\frac{n\pi k}{N+1}\right),\quad k=1,2,\ldots,N \tag{32}$$

with the associated first order energies, given by Eq. (24), with the exciton dispersion,

$$\tilde{J}_k=2J_0\cos\left(\frac{\pi k}{N+1}\right). \tag{33}$$

Here, J_0 is the nearest-neighbor interaction. Hence, the lowest energy (emitting) exciton has $\bar{k}=N$ for $J_0>0$, as is the case for the H-like aggregates considered here.

The coherence function can be easily obtained by inserting the zero order wave function coefficients from Eq. (32) into Eq. (26). The sum can be performed exactly, yielding

$$C^{(\mathrm{em})}(s)=\frac{e^{-\lambda^2}(-1)^s}{N+1}\{(N-s)\cos(\alpha s)+\sin[\alpha(s+1)]/\sin\alpha\},\quad W\ll\omega_0 \tag{34}$$

with $\alpha\equiv\pi/(N+1)$. The coherence function is plotted in Fig. 11(a), alongside the exact (nonperturbative) solution from Fig. 8 ($\sigma=0$ curve). The two functions are very similar. The main difference is in the amplitude of the oscillations which is smaller in the perturbative solution of Eq. (34). When $s=0$, the latter yields $C^{(\mathrm{em})}(0)=e^{-\lambda^2}$, a result that is *independent* of the nature of the excitonic coupling (i.e., nearest neighbor versus extended), as can easily be appreciated from Eq. (26) which reduces to a normalization condition when $s=0$. When W increases beyond the perturbation regime the emitting exciton becomes increasingly "free" from nuclear

dressing, causing $C^{(\mathrm{em})}(0)$ to exceed $e^{-\lambda^2}$. In our simulated MOPV4 helices the increase is about 28%.

The derivation of $g_{\mathrm{lum}}^{0\text{-}0}$ from Eq. (28) using Eqs. (34) and (25) is tedious and the result for arbitrary N is quite cumbersome. However, when N is sufficiently large (>10), the result simplifies considerably, reducing to

$$g_{\mathrm{lum}}^{0\text{-}0} = -kd\left\{(N+1)\cot\frac{(N+1)\phi}{2} + 2\tan\frac{\phi}{2}\right\}. \tag{35}$$

Equation (35) is almost identical to Eq. 21 in Ref. 33 derived using periodic boundary conditions and corrects a sign error. With the definition of ϕ given here ($\phi>0$ for a left-handed helix), Eq. 21 in Ref. 33 should also contain a negative sign as appears in Eq. (35).

The dependence of $g_{\mathrm{lum}}^{0\text{-}0}$ on N predicted by Eq. (35) is plotted in Fig. 11(b), alongside the exact (nonperturbative) numerical solution from Sec. III which also includes extended interactions. The two curves are quite similar due to the very weak dependence of $g_{\mathrm{lum}}^{0\text{-}0}$ on excitonic interactions, as seen in Eqs. (28) and (35) and remarked upon earlier.[33] Hence, Eq. (35) is an excellent approximation to $g_{\mathrm{lum}}^{0\text{-}0}$ in disorder-free helices even outside the perturbation regime. Equation (35) also explains the origin of the unphysical divergences seen in Fig. 10(b) (inset) which occur whenever the helix (approximately) makes an integer number of complete turns,[33]

$$(N+1)\phi \approx 2\pi l \quad (l=0,1,2,\ldots). \tag{36}$$

The divergence in $g_{\mathrm{lum}}^{0\text{-}0}$ occurs because the 0-0 transition becomes optically forbidden when condition (36) is satisfied exactly. This can be readily appreciated by evaluating the 0-0 line strength in Eq. (25) using the coherence function [Eq. (34)]. After some lengthy algebra, we obtain

$$I^{0\text{-}0} = I_{\mathrm{SM}}^{0\text{-}0}\frac{2}{N+1}\frac{\sin^2[(N+1)\phi/2]}{(\cos\phi+\cos\alpha)^2}\sin^2\alpha \tag{37}$$

with $\alpha \equiv \pi/N+1$. The right-hand side of Eq. (37) is negligible under condition (36) which includes the achiral H-aggregate limit ($\phi=0$). The fact that $I^{0\text{-}0}$ can be nullified while the replica intensities cannot, see Eq. (27), is due to the coherent nature of 0-0 emission. In Ref. 33, the divergence in $g_{\mathrm{lum}}^{0\text{-}0}$ is shown to disappear when corrections of order $\mathrm{O}[kR_{mn}]$ are included in the excitonic couplings. (R_{mn} is the distance between chromophores m and n.)

Finally, using Eq. (29), the replica dissymmetries for nearest-neighbor coupling and open boundary conditions become (for $N\gg 1$)

$$g_{\mathrm{lum}}^{0\text{-}\nu_t} = -4kd\Gamma(\nu)J_0\sin\phi, \quad \nu_t \geqslant 1. \tag{38}$$

Equation (38) is a substantial improvement over the analogous expression derived in Ref. 33 using periodic boundary conditions. Eq. (38) is, in fact, identical to the first term in Eq. (26) of Ref. 33. However, the second term in Eq. (26) (of Ref. 33) is an artifact due to the periodic boundary conditions, causing unphysical oscillations in $g_{\mathrm{lum}}^{0\text{-}\nu_t}$ as a function of N.

VI. DISCUSSION/CONCLUSION

In MOPV4 helical aggregates, the localizing influences of disorder and vibronic coupling compete with the delocalizing influence of energy transfer to create complex photophysical behaviors. To better understand the unusual spectral dependence of the CPL dissymmetry $g_{\mathrm{lum}}(\omega)$ measured in dilute solutions of MOPV4 helices, and in particular, the surge in $g_{\mathrm{lum}}(\omega)$ near the 0-0 transition,[11] we expressed the 0-0 dissymmetry $g_{\mathrm{lum}}^{0\text{-}0}$ and the PL 0-0 line strength $I^{0\text{-}0}$ entirely in terms of the luminescing exciton's coherence function, $\langle C^{(\mathrm{em})}(s)\rangle$. The relationship was investigated numerically using full-scale simulations based on a Gaussian distribution of transition frequencies and analytically in the limit of weak disorder.

The spectral shape of $g_{\mathrm{lum}}(\omega)$ in MOPV4 helices reveals information about the anatomy of the emitting excitonic polaron. The delocalization of the vibronically excited polaronic "center," described by the coherence function $\langle C^{(\mathrm{em})}(s)\rangle$, dictates the magnitude of $g_{\mathrm{lum}}(\omega)$ in the vicinity of the 0-0 emission frequency, while the polaron radius dictates the magnitude of $g_{\mathrm{lum}}(\omega)$ in the spectral region corresponding to the sidebands (0-1, 0-2,…).[11] With respect to the multiparticle expansion of the emitting polaron, $g_{\mathrm{lum}}^{0\text{-}0}$ depends only on the vibronic (single-particle) coefficients, whereas all sideband dissymmetries, $g_{\mathrm{lum}}^{0\text{-}\nu_t}$ ($\nu_t \geqslant 1$) require products of vibronic/vibrational (two-particle) and single-particle coefficients. Hence, were it not for the two-particle contributions present in the emitting polaron in Eqs. (3) and (23), the polaron radius along with the sideband dissymmetries would rigorously vanish.[11,33] Except for the somewhat pathological limit of very slight intra-aggregate disorder (small σ and/or large l_0) discussed at length below, $|g_{\mathrm{lum}}^{0\text{-}0}|$ increases with the exciton coherence length, while the sideband dissymmetries increase with polaronic radius. Hence, it becomes possible to extract important polaronic parameters from measured spectra.

The present work focuses mainly on interpreting the 0-0 portion of the emission spectrum. In particular we are interested in how the high-energy surge in $|g_{\mathrm{lum}}(\omega)|$ relates to the exciton coherence length that, in turn, depends on the degree of disorder. For chiral aggregates, the 0-0 dissymmetry using Eqs. (18b) with (20) is given by

$$g_{\mathrm{lum}}(\omega=\omega_{\mathrm{peak}}^{0\text{-}0}) \approx \langle g_{\mathrm{lum}}^{0\text{-}0}\rangle = \frac{kd\sum_s \langle C^{(\mathrm{em})}(s)\rangle s\sin(\phi s)}{\sum_s \langle C^{(\mathrm{em})}(s)\rangle\cos(\phi s)}, \tag{39}$$

where the numerator and denominator represent the rotational strength $\langle R_{\mathrm{lum}}^{0\text{-}0}\rangle$ and PL line strength $\langle I^{0\text{-}0}\rangle$, respectively. In the limit of strong disorder, $\langle g_{\mathrm{lum}}^{0\text{-}0}\rangle$ tends to zero and $\langle I^{0\text{-}0}\rangle$ approaches its isolated molecule value ($e^{-\lambda^2}$), reflecting localization on a single site. As the disorder is reduced, the exciton's coherence range expands (see Fig. 8) driving $|\langle g_{\mathrm{lum}}^{0\text{-}0}\rangle|$ sharply upward. The increase is fueled primarily by a precipitous drop in $\langle I^{0\text{-}0}\rangle$ due to increasingly efficient destructive interferences embodied in the denominator of Eq. (39) as the exciton wave expands. Less efficient destructive

interferences also appear in the numerator of Eq. (39) due to the longer range of $s\sin(\phi s)$ compared with $\cos(\phi s)$. The overall effect is a marked increase in $|\langle g_{\mathrm{lum}}^{0\text{-}0}\rangle|$ as disorder vanishes. By contrast, the sideband dissymmetries are far less sensitive to disorder (see Fig. 6) and the exciton coherence length. A detailed analysis of spectral shape of $g_{\mathrm{lum}}(\omega)$ and $S(\omega)$ in dilute MOPV4 solutions (see Fig. 3) conducted in Ref. 11 yielded a disorder width of $\sigma=0.12$ eV, and a spatial correlation length, $l_0=4-5$ molecules, exceeding the exciton coherence length of approximately 2–3 molecules.[11] In achiral aggregates, where $g_{\mathrm{lum}}(\omega)$ is zero, information on the spatial correlation length and exciton coherence size can be extracted solely from the ratio of the 0-0 to 0-1 PL intensities. Such an analysis was conducted in polythiophene π-stacks, where the spatial correlation length was estimated to emcompass several sites.[16]

In the very weak disorder limit described by condition (15), $\langle g_{\mathrm{lum}}^{0\text{-}0}\rangle$ can undergo a sign reversal dictated by the number of chromophores N comprising the helix. In this limit, the behavior of $\langle g_{\mathrm{lum}}^{0\text{-}0}\rangle$ scales nonlinearly with the helical length (or N), as demonstrated in Fig. 10(b). For a left (right)-handed helix of arbitrary N, $\langle g_{\mathrm{lum}}^{0\text{-}0}\rangle$ is initially negative (positive) for strong disorder, as the exciton coherence is limited to only $N_{\mathrm{coh}}=1-2$ chromophores. Figure 10(b) shows that as the weak disorder limit is approached (and N_{coh} approaches N) the sign of $\langle g_{\mathrm{lum}}^{0\text{-}0}\rangle$ changes for helices which are between $n+\frac{1}{2}$ and $n+1$ complete turns ($n=0,1,\ldots$). Since the side band dissymmeries are sign-stable, the resulting CPL dissymmetry spectrum, $g_{\mathrm{lum}}(\omega)$, changes sign near the 0-0 transition.

The possibility of observing this intriguing size and disorder-induced change in the handedness of the 0-0 emitted light requires low temperatures to ensure emission originates from the lowest energy exciton. For $W=0.15$ eV, as is appropriate for MOPV4 helices, the approximate spacing between the lowest two excitons in a defect-free aggregate of 12 chromophores (the minimum N to observe the sign change) is $\approx 80\ \mathrm{cm}^{-1}$. Hence, the temperature should be substantially less than 120 K to observe the sign reversal. Unfortunately, the number of 0-0 photons emitted is not large, approximately 1000 times fewer compared to single molecule emission (see Fig. 6). Of course, the actual number of 0-0 photons depends on the pump power, competing nonradiative rates, etc., but should be within detectable levels.

The modulation $s\sin\phi s$ which appears in the rotational line strength [see Eq. (20)] arises from the term, $\boldsymbol{\mu}_n \times \boldsymbol{\mu}_{n+s}\cdot(\mathbf{r}_n-\mathbf{r}_{n+s})$, intrinsic to expressions for circularly polarized emission or absorption,[40] after inserting the *radially* directed transition dipole moments. The long-range modulation not only leads to the aforementioned 0-0 dissymmetry sign change, but is also responsible for the strong sensitivity of $g_{\mathrm{lum}}(\omega)$ to extended excitonic interactions [see Eq. (31) and inset of Fig. 2]. Hence, careful analysis of the frequency dependence of $g_{\mathrm{lum}}(\omega)$ can provide a valuable check for calculations of extended intermolecular interactions in the condensed phase, including the important effects of dielectric screening.

In the current work, only site-disorder is considered although in general there may also be important contributions from off-diagonal disorder through random variations in the transfer integrals, J_{mn}. A more sophisticated model might also include a Gaussian distribution of J_{mn} values, with a width σ_{od} and perhaps also correlation to the offsets Δ_m and Δ_n. We are currently investigating the role of off-diagonal disorder alone on localization and the exciton coherence function and whether such a model can reproduce all of the photophysical observables with the same level of success as that achieved with the current diagonal disorder model.

Finally, the analysis of Sec. V assumes weak excitonic coupling (W) in relation to the EP coupling, $W \ll \lambda^2\omega_0$. The opposite limit of strong excitonic coupling has been treated in Ref. 33. Although the 0-0 dissymmetry remains remarkably insensitive to exciton bandwidth the side band CPL dissymmetries increase rapidly with W becoming comparable to the 0-0 dissymmetry when $W \gg \lambda^2\omega_0$. In the current view, this is understood as an increase in the polaron radius as the emitting excitation approaches the BO product of a free exciton and a free phonon. In future work, we will further develop the relationship between the polaron structure and the sideband CPL dissymmetries. Eventually, we would like to utilize the multiparticle basis set to investigate polaron dynamics along the helical axis.[8–10] The time scale of intraband relaxation should depend strongly on the coupling of the exciton to the nuclear framework over which it travels, i.e., there should be an important distinction between polaron transport versus free exciton transport.

ACKNOWLEDGMENTS

The work at Temple is supported by the National Science Foundation under Grant No. DMR-0606028. The work in Mons is partly supported by the Interuniversity Attraction Pole program of the Belgian Federal Science Policy Office (PAI 6/27) and by FNRS-FRFC. E.H. and D.B. are postdoctoral researcher and research director of FNRS. The research work in Eindhoven was supported by the Netherlands Organization for Scientific Research (NWO) through a grant in the VIDI program. The authors thank Dr. A. P. H. J. Schenning and Dr. P. Jonkheijm for generous supply of the MOPV4 material and their help with the spectroscopic measurements.

[1] A. P. H. J. Schenning and E. W. Meijer, Chem. Commun. (Cambridge) **2005**, 3245.
[2] A. P. H. J. Schenning, P. Jonkheijm, E. Peeters, and E. W. Meijer, J. Am. Chem. Soc. **123**, 409 (2001).
[3] P. Jonkheijm, F. J. M. Hoeben, R. Kleppinger, J. van Herrikhuyzen, A. P. H. J. Schenning, and E. W. Meijer, J. Am. Chem. Soc. **125**, 15941 (2003).
[4] F. J. M. Hoeben, L. M. Herz, C. Daniel, P. Jonkheijm, A. P. H. J. Schenning, C. Silva, S. C. J. Meskers, D. Beljonne, R. T. Phillips, R. H. Friend, and E. W. Meijer, Angew. Chem., Int. Ed. **43**, 1976 (2004).
[5] P. Prins, K. Senthilkumar, F. C. Grozema, P. Jonkheijm, A. Schenning, E. W. Meijer, and L. D. A. Siebbeles, J. Phys. Chem. B **109**, 18267 (2005).
[6] C. Jeukens, P. Jonkheijm, F. J. P. Wijnen, J. C. Gielen, P. C. M. Christianen, A. Schenning, E. W. Meijer, and J. C. Maan, J. Am. Chem. Soc. **127**, 8280 (2005).
[7] P. Jonkheijm, P. van der Schoot, A. Schenning, and E. W. Meijer, Science **313**, 80 (2006).
[8] L. M. Herz, C. Daniel, C. Silva, F. J. M. Hoeben, A. P. H. J. Schennnig, E. W. Meijer, R. H. Friend, and R. T. Phillips, Phys. Rev. B **68**, 045203 (2003).
[9] D. Beljonne, E. Hennebicq, C. Daniel, L. M. Herz, C. Silva, G. D.

Scholes, F. J. M. Hoeben, P. Jonkheijm, A. P. H. J. Schenning, S. C. J. Meskers, R. T. Phillips, R. H. Friend, and E. W. Meijer, J. Phys. Chem. B **109**, 10594 (2005).
[10] C. Daniel, S. Westenhoff, F. Makereel, R. H. Friend, D. Beljonne, L. M. Herz, and C. Silva, J. Phys. Chem. C **111**, 19111 (2007).
[11] F. C. Spano, S. C. J. Meskers, E. Hennebicq, and D. Beljonne, J. Am. Chem. Soc. **129**, 7044 (2007).
[12] B. M. W. Langeveld-Voss, D. Beljonne, Z. Shuai, R. A. J. Janssen, S. C. J. Meskers, E. W. Meijer, and J. L. Bredas, Adv. Mater. (Weinheim, Ger.) **10**, 1343 (1998).
[13] G. Lakhwani, G. Koeckelberghs, S. C. J. Meskers, and R. A. J. Janssen, Chem. Phys. Lett. **437**, 193 (2007).
[14] S. C. J. Meskers, E. Peeters, B. M. W. Langeveld-Voss, and R. A. J. Janssen, Adv. Mater. (Weinheim, Ger.) **12**, 589 (2000).
[15] B. M. W. Langeveld-Voss, R. A. J. Janssen, and E. W. Meijer, J. Mol. Struct. **521**, 285 (2000).
[16] F. C. Spano, J. Chem. Phys. **122**, 234701 (2005).
[17] E. O. Potma and D. A. Wiersma, J. Chem. Phys. **108**, 4894 (1998).
[18] H. Fidder, J. Knoester, and D. A. Wiersma, Chem. Phys. Lett. **171**, 529 (1990).
[19] *J-aggregates*, edited by T. Kobayashi (World Scientific, Singapore, 1996).
[20] C. C. Wu, M. C. Delong, Z. V. Vardeny, and J. P. Ferraris, Synth. Met. **137**, 939 (2003).
[21] P. F. van Hutten, J. Wildeman, A. Meetsma, and G. Hadziioannou, J. Am. Chem. Soc. **121**, 5910 (1999).
[22] W. Porzio, S. Destri, M. Mascherpa, and S. Bruckner, Acta Polym. **44**, 266 (1993).
[23] T. Siegrist, C. Kloc, R. A. Laudise, H. E. Katz, and R. C. Haddon, Adv. Mater. (Weinheim, Ger.) **10**, 379 (1998).
[24] M. Muccini, M. Schneider, C. Taliani, M. Sokolowski, E. Umbach, D. Beljonne, J. Cornil, and J. L. Bredas, Phys. Rev. B **62**, 6296 (2000).
[25] F. Meinardi, M. Cerminara, A. Sassella, A. Borghesi, P. Spearman, G. Bongiovanni, A. Mura, and R. Tubino, Phys. Rev. Lett. **89**, 157403 (2002).
[26] W. Gebauer, A. Langner, M. Schneider, M. Sokolowski, and E. Umbach, Phys. Rev. B **69**, 1254201 (2004).
[27] F. Meinardi, M. Cerminara, A. Sassella, R. Bonifacio, and R. Tubino, Phys. Rev. Lett. **91**, 247401 (2003).
[28] F. C. Spano, Annu. Rev. Phys. Chem. **57**, 217 (2006).
[29] F. C. Spano, J. Chem. Phys. **116**, 5877 (2002).
[30] F. C. Spano, Phys. Rev. B **71**, 235208 (2005).
[31] F. C. Spano, J. Chem. Phys. **118**, 981 (2003).
[32] C. Didraga and J. Knoester, J. Chem. Phys. **121**, 10687 (2004).
[33] F. C. Spano, Z. Zhao, and S. C. J. Meskers, J. Chem. Phys. **120**, 10594 (2004).
[34] A sign error in the reported pitch angle was corrected in an erratum to Ref. 11; see J. Am. Chem. Soc. **129**, 16278E (2007).
[35] E. W. Knapp, Chem. Phys. **85**, 73 (1984).
[36] J. Cornil, D. Beljonne, C. M. Heller, I. H. Campbell, B. K. Laurich, D. L. Smith, D. D. C. Bradley, K. Mullen, and J. L. Bredas, Chem. Phys. Lett. **278**, 139 (1997).
[37] P. O. J. Scherer and S. F. Fischer, Chem. Phys. Lett. **86**, 269 (1984).
[38] M. R. Philpott, J. Chem. Phys. **55**, 2039 (1971).
[39] Reference 11 includes an approximate form of the cubic frequency factor in defining the emission spectrum but the more accurate form reported here was actually used in all numerical calculations. However, using the approximate leads to negligible effects.
[40] A. Rodger and B. Norden, *Circular Dichroism and Linear Dichroism* (Oxford University Press, Oxford, 1997).
[41] The vertical transition frequency arises when converting the transition matrix element of the momentum operator (which appears in the magnetic dipole moment operator) to the matrix element of the electric dipole moment operator. In Ref. 34, we used the 0-0 transition frequency as an approximation, although the vertical transition frequency includes also the nuclear relaxation energy. The latter is approximately 0.2 eV for the ring breathing mode in MOPV*n*.
[42] T.-Q. Nguyen, I. B. Martini, J. Liu, and B. J. Schwartz, J. Phys. Chem. B **104**, 237 (2000).
[43] B. J. Schwartz, Annu. Rev. Phys. Chem. **54**, 141 (2003).
[44] F. C. Spano, Chem. Phys. **325**, 22 (2006).
[45] J. Clark, C. Silva, R. H. Friend, and F. C. Spano, Phys. Rev. Lett. **98**, 206406 (2007).